T. Joshua Pfefer
Bernard Choi
Gracie Vargas
Karen M. McNally
A. J. Welch

Biomedical Engineering Program,
The University of Texas at Austin,
Austin, TX 78712

Pulsed Laser-Induced Thermal Damage in Whole Blood

An investigation of the effects of laser irradiation with a wavelength of 532 nm and pulse duration of 10 ms on whole blood was performed in vitro. Threshold radiant exposures for coagulation were quantified and transient radiometric temperatures were measured. The progression of effects with increasing radiant exposure—from evaporation to coagulation-induced light scattering to aggregated coagulum formation to ablation—is described. Results indicate that coagulation and ablation occur at temperatures significantly in excess of those assumed in previous theoretical studies. An Arrhenius rate process analysis based on hemoglobin data indicates good agreement with experimental results. [S0148-0731(00)00902-X]

1 Introduction

Thermal coagulation of blood constituents may play a significant role in a variety of therapeutic laser applications such as the selective destruction of vessels in the skin [1], retina [2], and gastrointestinal tract [3], as well as tissue welding [4] and achieving hemostasis [5]. However, there remains a lack of quantitative data regarding optical and thermal effects of blood photocoagulation, particularly for laser pulses on the order of tens of milliseconds or less.

Laser-induced blood vessel necrosis, or selective photothermolysis, typically involves the absorption of light by hemoglobin (Hb), the diffusion of heat through the blood, vessel wall, and perivascular dermis, with the goal of selectively coagulating endothelial cells and/or blood constituents. In recent studies using optical coherence tomography (OCT) [6] and confocal microscopy [7], pulsed laser irradiation has been shown to produce coagula in the lumen of cutaneous vessels in vivo. As radiant exposure (H_o) levels increase, these coagula increase in size, filling the lumen and causing vessel occlusion, which can lead to necrosis. These results, and the inability of present optical-thermal models to predict them, underscore the need for a greater understanding of the effect of pulsed laser irradiation on blood.

1.1 Background. Blood plasma is comprised primarily of water (91 percent) and proteins (7 percent, 7.3 gm/dL) such as albumin (4.5 gm/dL) and globulin (2.5 g/dL) [8,9]. The primary protein component of the erythrocytes is hemoglobin (14–16 gm/dL of whole blood), although a smaller quantity of proteins such as spectrin comprise the cell membranes.

Thermally induced biochemical and morphological effects in blood have been investigated previously. As blood is exposed to heat, the normally biconcave red blood cell assumes a biconvex shape, then forms a spherocyte [10]. Partial membrane fragmentation occurs, resulting in a loss of hemoglobin. Finally, the membrane disintegrates into globules, which aggregate to form a mesh, and the release of hemoglobin is completed [11,12]. The thermal damage to the membrane is attributed to conformational changes in erythrocyte membrane structural proteins [13]. These alterations have been shown to induce an increase in scattering (at $\lambda=632$ and 1064 nm) and absorption (at $\lambda=586$ and 1064 nm), although the change in absorption may result from de-oxygenation of hemoglobin, and thus be highly wavelength-dependent [10,14,15].

Several in vitro studies involved continuous wave (CW) irradiation of whole blood, blood constituents, or phantoms. Early studies centered on the effect of CW laser radiation on morphological changes in erythrocytes and the release of hemoglobin [11,16,17]. Halldorsson [15] recorded temperatures with a thermal camera during CW Nd:YAG laser irradiation of whole blood. This study indicated that evaporation played a significant role in surface heat loss and coagulum formation.

Verkruysse et al. [14] documented changes in transmission and reflection of pulsed dye laser light ($\lambda=586$ nm), which they attributed to temperature-dependent variations in absorption. Other recent studies documented the development of pulsed laser-induced coagulation in albumen—essentially a water-ovalbumin (86-14 percent) solution [18,19]. In these investigations, thermal damage produced an increase in light scattering and a coagulum which, for higher radiant exposures, adhered to the optical fiber tip. It should be noted that albumin has been used as a thermally activated adhesive in ''laser-tissue welding'' studies [4,20].

1.2 Predicting Thermal Damage in Blood. The standard method of mathematically quantifying thermal damage in biological tissue involves using the Arrhenius rate process equation, which describes a unimolecular rate process [21–23]:

$$\Omega(t)=\ln\left(\frac{C(0)}{C(t)}\right)=A\int_0^t \exp\left(-\frac{E_a}{RT(t)}\right)d\tau \tag{1}$$

where Ω is the thermal damage coefficient (dimensionless), C is the concentration of molecules in the native state, t is time (s), A is the frequency factor (1/s), E_a is the activation energy (J/mole) required to initiate the chemical transformation (protein denaturation), R is the universal gas constant (8.31 J/mole/K), and T is temperature (K). The damage threshold for tissue necrosis is commonly selected as $\Omega=1.0$ (a damage concentration of 63 percent for a unimolecular system). When performing an Arrhenius analysis, the threshold is assumed to correspond with an experimental endpoint—typically a visible increase in light scattering, which makes the tissue appear white [24]. It should be noted that this technique may yield differing results depending on the endpoint and detection method used.

Rate process coefficients for blood constituents, bulk skin, and arterial tissue from the literature are presented in Table 1, along with the threshold temperatures for coagulation (T_{th}), for a 10 ms step change in temperature. These data were calculated using the following relation derived from Eq. (1):

$$T_{th}=\frac{E_a}{R(\ln A+\ln t)} \tag{2}$$

The relationship between T_{th} and temperature step duration is also graphed in Fig. 1 for selected tissue property data from Table 1.

Previous theoretical models of vascular lesion treatment have generally assumed threshold blood coagulation temperatures of

Contributed by the Bioengineering Division for publication in the JOURNAL OF BIOMECHANICAL ENGINEERING. Manuscript received by the Bioengineering Division June 14, 1999; revised manuscript received November 18, 1999. Associate Technical Editor: M. Toner.

Table 1 Arrhenius rate process coefficients of blood constituents and related biological materials and corresponding threshold temperatures calculated for a 10 ms, constant-temperature exposure. Asterisks indicate E_a determined from data in the present study.

Material	A(1/s)	E_a (kJ/mole)	T_{th}(°C) for τ=10 ms	Source
1. Bulk skin	3.1×10^{98}	628	67	[25]
2. Arterial tissue	5.6×10^{63}	430	91	[35]
3. Erythrocyte membrane	6.8×10^{36}	249	160	[36]
4. Erythrocyte membrane	10^{31}	212	109	[17]
5. Bovine serum albumin	3.2×10^{56}	379	90	[20]
6. Ovalbumin	3.8×10^{57}	385	89	[25]
7. Hemoglobin	7.6×10^{76}	550	100	[37]
8. Hemoglobin	7.6×10^{66}	455	93	[13]
9. Whole blood	7.6×10^{66}	434	76	*(H_{th}=3.6 J/cm^2)
10. Whole blood	7.6×10^{66}	448	88	*(H_{th}=4.4 J/cm^2)

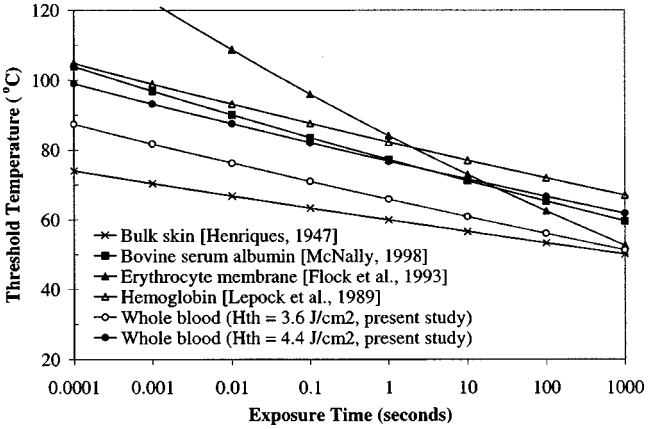

Fig. 1 Threshold temperatures of skin and blood constituents as a function of exposure time, using Eq. (2), the rate process data in Table 1, and assuming step changes in temperature. Symbols are for identification purposes only and do not represent specific data points.

60°C–80°C. These values are based on studies involving exposure durations on the order of seconds or greater and a study of porcine bulk skin burns [25], which is commonly cited in the literature [1,26,27]. Therefore, the purpose of this is study to investigate the validity of these threshold temperatures and rate process coefficients through quantification of the thermal and optical effects of pulsed laser-induced irradiation of blood.

2 Materials and Methods

The experimental portion of this study involved the use of three primary methods: thermal imaging (for transient surface temperatures), optical coherence tomography (for coagulum morphology, particularly thickness), and laser transmission measurements. All irradiations were performed with a Coherent Versapulse VPW-a clinical KTP (frequency doubled Nd:YAG) laser with a wavelength of 532 nm. A pulse duration (τ_p) of 10 ms and beam diameters of 5 mm (H_o=2.5–6.0 J/cm^2), 4 mm (H_o =6.5–7.5 J/cm^2), and 3 mm (H_o=8.0–13.0 J/cm^2) were used. Human venous blood from a healthy male donor was withdrawn and placed in vials containing the anti-coagulant ethylenediamine tetraacetic acid (EDTA). While EDTA prevents the (nonthermal) blood coagulation process—a cascade of chemical reactions involving clotting factors and fibrin formation that occurs over several seconds—it has not been noted to have any effect on heat-induced denaturation in blood proteins [14,10]. When necessary, vials were placed in a refrigerator for overnight storage and returned to ambient temperature the following day. All blood was used within 36 hours of withdrawal. Gentle agitation was performed to achieve a homogeneous distribution of blood constituents. For open-cuvette irradiations, blood was mixed in the vial, dispensed to the cuvette, and irradiated within 30 s. For spectrophotometer (glass) cuvette irradiations, blood was agitated within the closed cuvette immediately before irradiation.

Data have not been corrected for losses due to specular reflection. For the thermal imaging setup, the handpiece was oriented at an incident angle of ~22 deg (from perpendicular) and an open cuvette was used (n_{air}=1.0, n_{blood}=1.33), thus producing specular reflection of 2.0 percent. For OCT imaging and transmission measurements, the incident angle was 0 deg, and an enclosed cuvette was used, resulting in a specular reflection of 4.3 percent (air–glass and glass–blood interfaces, where n_{glass}=1.5).

2.1 Thermal Imaging and Thermal Damage Calculations. Radiometric temperature measurements were performed using an Inframetrics 600L (λ=3–5 μm, band-limited) thermal camera. Radiation emitted from a sample (or the blackbody) was reflected off of a standard first-surface mirror to accommodate a horizontally oriented detector. Calibration curves for several temperature ranges were obtained using a variable temperature blackbody (Ealing Electro-Optics, Model BB1001-67). When recording high radiant exposure events, the camera was set for wider temperature ranges, thus necessitating the use of calibration curves, which maximized the accuracy at high temperatures at the expense of accuracy at lower temperatures. The spatial resolution of the camera was approximately 0.1 mm. In calculating temperature from the measured emissive power, the emissivity of blood was assumed to be equal to that of water (ε=0.96).

Temperature measurements through the center of the beam spot were taken using the camera's line-scan mode. This method provided acquisition of a single line of spatial data at a rate of 8 kHz, and thus a temporal resolution of 125 μs. However, the line scan mode also introduced several problems that limited the continuity of measurement: The scale bar and time code, which could not be removed from the video display, blocked several lines of data; fly-back in the camera resulted in a loss of 3.5 ms of data for every field (each 16.5 ms). Thus, transient temperature distributions at the center of the beam were measured in temporal segments and a continuous data set was reconstructed by averaging data from several discontinuous events.

Quantitative estimation of thermal damage was achieved by evaluating the Arrhenius equation using radiometric temperature data and rate process coefficients for bulk skin [25] and Hb [13]. Numerical integration of this relation was performed at each 125-μs time step using the trapezoidal method.

2.2 Optical Coherence Tomography Imaging. An OCT system used previously to image thermal injury in hamster blood vessels in vivo [6] was used to determine the macroscopic morphology of coagula. The system consisted of a modified Michelson interferometer that measured the intensity of light backscattered from specific locations within the sample. The optical source was a 1280 nm center wavelength superluminescent diode. A single depth scan was acquired by changing the reference arm length. Scanning mirrors were used to scan the beam laterally across the sample in order to construct a two dimensional cross-sectional image. The OCT system had a high dynamic range (>100 dB) and a spatial resolution of ~20 μm, laterally and axially.

Blood was enclosed in a glass spectrophotometer cuvette (2 mm sample path length), agitated, then irradiated. Immediately after irradiation the sample was moved to the OCT stage and a two-dimensional image was generated. The acquisition time for an image consisting of 200 depth scans was approximately 20 s.

2.3 Transmission Measurements. Transmission measurements were performed to quantify the effect of laser-induced optical changes. The glass spectrophotometer cuvette was filled with blood. A photodetector below the cuvette recorded the intensity of the alignment beam ($\lambda=635$ nm). A circular aperture 6 mm in diameter was placed between the cuvette and the photodetector to remove highly scattered light. The output from the photodiode was captured by a digital oscilloscope (Tektronix TDS 640A) and transferred by disk from the oscilloscope to a personal computer.

Although a high-pass filter was used to minimize the effect of the KTP laser and flash lamp, the signal from the alignment beam was overwhelmed by stray light during the laser pulse, making it impossible to obtain transient data during the pulse. Therefore, the intensity of transmitted light at $\lambda=635$ nm was measured before and after the KTP laser pulse. These two values were compared to determine the change in transmission due to coagulation.

3 Results

3.1 Observations During Open-Cuvette Irradiations. As the radiant exposure was increased from 2.5 J/cm^2 (for a pulse duration of 10 ms), no visible changes were noted until 3.6 J/cm^2, when the blood surface appeared to be slightly discolored (whitened). At $H_o=4.4$ J/cm^2 a thin, light-gray disk about 8 mm in diameter, consisting of fine particles (coagulated blood components), was produced. The disk became irregular as it dispersed, and appeared to dissolve when the cuvette was agitated. For $H_o>4.4$ J/cm^2, this disk became increasingly visible, then began to aggregate at a radiant exposure of 8.0 J/cm^2. At $H_o=10$ J/cm^2, the thin ($\sim$100 μm) coagulum could be removed from the cuvette with forceps. Although ablation—explosive vaporization identified by an audible acoustic transient (popping sound) [14] and fragmentation of the otherwise disk-shaped coagulum—was noted at $H_o=11$ J/cm^2, it did not occur with every pulse until $H_o=13$ J/cm^2. Ablation typically involves vapor-pressure-driven bubble expansion and subsequent collapse, both of which can cause material ejection or other forms of mechanical damage. Limited experimental data were collected for radiant exposures greater than 10 J/cm^2 due to the occurrence of ablation events that caused adverse results such as cuvette fracture.

Nonablative evaporation was detected by suspending a glass slide $\sim$1 cm above the blood. As the radiant exposure increased, the first noticeable change (at $H_o=2.7$ J/cm^2) was an accumulation of a thin layer of condensation (clear liquid droplets assumed to be water) on the slide, appearing soon after the laser pulse and disappearing after a few seconds. The apparent thickness of the droplet layer increased steadily with H_o. An attempt to quantify blood mass loss due to evaporation, using a scale with sensitivity on the order of tens of micrograms, was unsuccessful due to a low signal to noise ratio.

3.2 Temperature Measurements and Damage Predictions. The temperature reconstructions for a point near the center of the beam are shown in Fig. 2. Each curve represents an average of data from 10–15 irradiations. The standard deviation for points near the temperature peak was $\pm$2°C for $H_o=3$ J/cm^2, increasing to $\pm$5°C at $H_o=12$ J/cm^2. Initially, the rate of temperature rise was proportional to the radiant exposure. For lower radiant exposures (3–5 J/cm^2), this rate did not change significantly unless temperatures exceeded 70°C. However, for higher radiant exposures (8–12 J/cm^2), deviation from the initial rate of temperature rise did not appear to be significant until temperatures approached 100°C.

Predictions of transient thermal damage accumulation based on Eq. (1) and using the temperature data in Fig. 2, and rate process parameters for Hb [13] and bulk skin [25] are presented in Figs. 3(*a*) and 3(*b*), respectively. These figures indicate similar trends, yet Fig. 3(*b*) indicates much earlier coagulation onset ($\Omega=1$) and greater damage levels than Fig. 3(*a*).

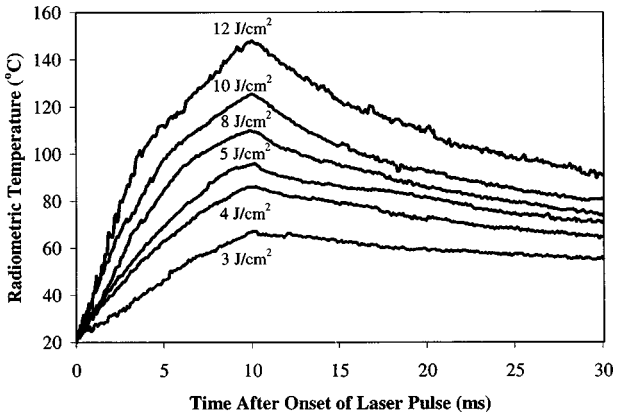

Fig. 2 Radiometric temperature distributions for a point near the center of the laser beam ($\lambda=532$; $\tau_p=10$ ms) for six different radiant exposure levels

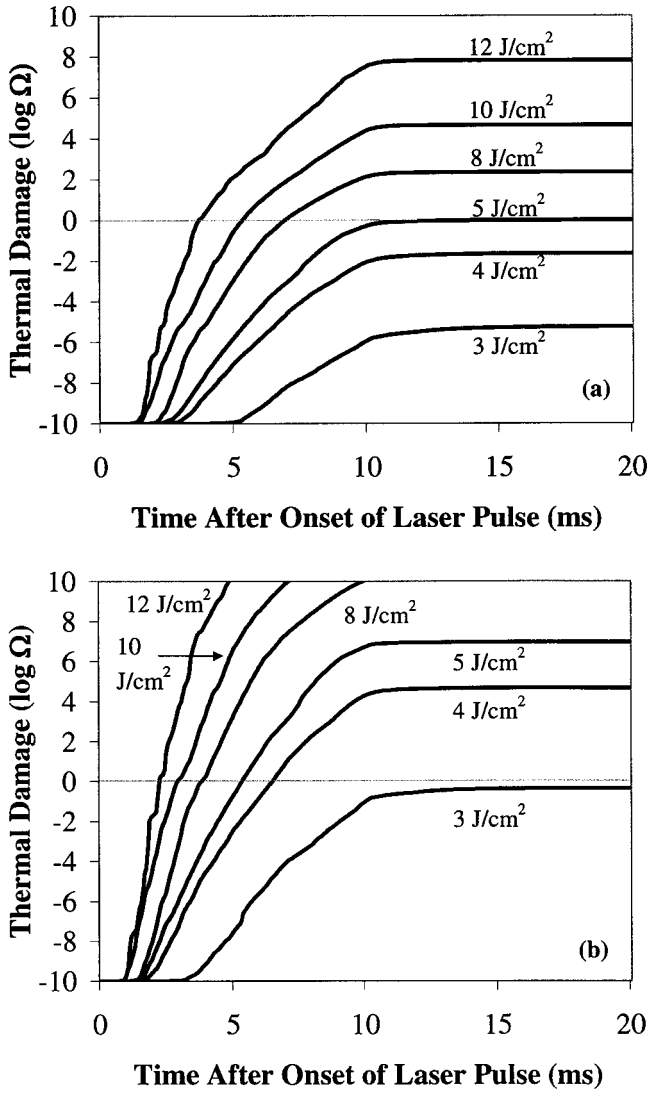

Fig. 3 Thermal damage levels calculated from radiometric temperature distributions (Fig. 2) using rate process coefficients for: (*a*) hemoglobin [13]; and (*b*) bulk skin [25]. Horizontal lines at $\Omega=1$ indicate the coagulation threshold. Note that minimum and maximum values of Ω (10^{-10} and 10^{10}) were chosen arbitrarily.

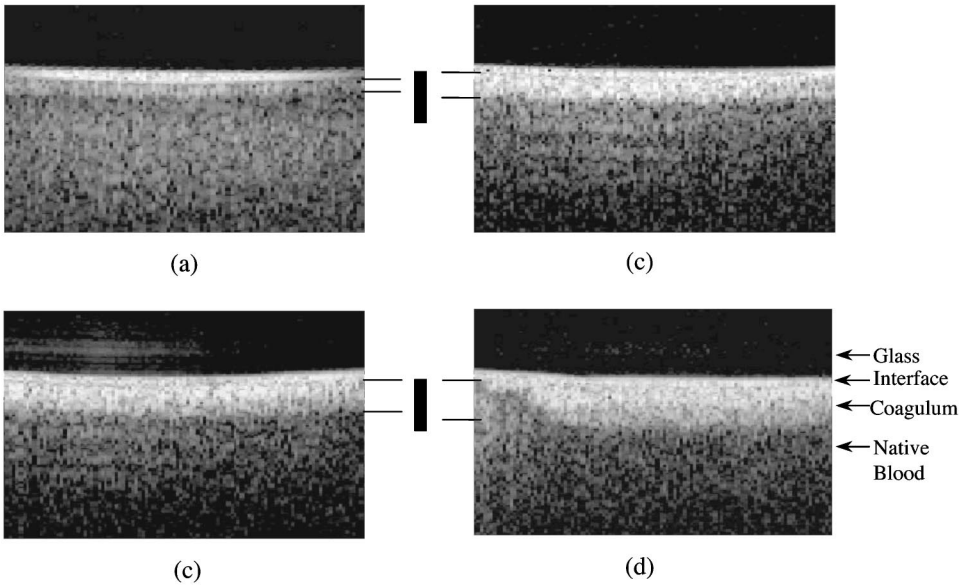

Fig. 4 OCT images documenting the morphology of coagulated regions of whole blood at radiant exposures of: (*a*) 4.4, (*b*) 6, (*c*) 8, and (*d*) 10 J/cm^2. As labeled in (*d*), four regions are visible (from top to bottom): glass (black), glass–blood interface (white), coagulated blood (bright speckle), and native blood (darker speckle). The length of size bars corresponds to a distance of approximately 200 μm. The thickness of each coagulum is indicated by a pair of thin lines. The left side of image (*d*) shows the edge of coagulum. Note that the intensity of the OCT signal in (*a*) is lower in the coagulum (and higher in the native blood) than in the corresponding regions of the other images.

3.3 Coagulum Morphology. Figure 4 shows a series of OCT images that document the change in coagulum thickness with increasing radiant exposure. In these images, four layers are visible (as labeled in Fig. 4(*d*), from top to bottom): a dark layer of glass, a thin white layer due to the change in index of refraction at the interface between the glass ($n=1.5$) and the blood ($n=1.33$), a light, speckled region of highly scattering coagulated blood, and a darker speckled region of native blood, which extends to the bottom of each image.

A set of three to five images at each radiant exposure ($\tau_p=10$ ms) was used to generate the graph of coagulum thickness as a function of radiant exposure presented in Fig. 5. The first measurable coagulum occurred at $H_o=4.4$ J/cm^2. The initial increase in coagulum thickness was followed by a regime of linear growth in coagulum size with radiant exposure. Due to the thickness of the coagula (<200 μm), the spatial resolution of the OCT system (~ 20 μm), and the high noise level associated with OCT imaging of scattering media, a high level of precision was difficult to obtain. This variability is indicated in Fig. 5 by the error bars ($\pm$standard deviation).

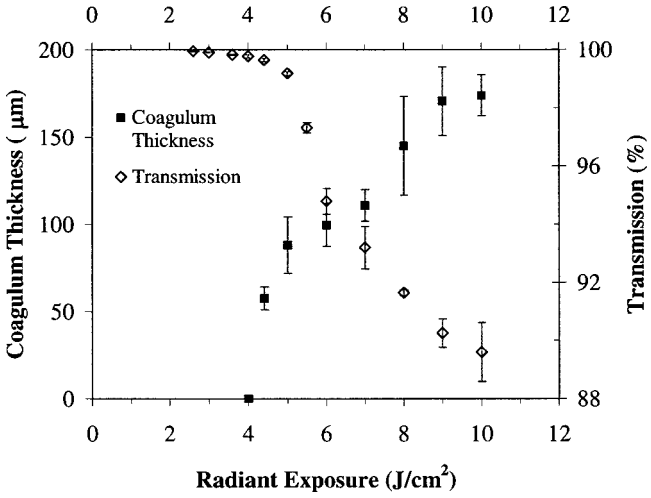

Fig. 5 The effect of increasing radiant exposure on coagulum thickness (from OCT images) and transmission of coaligned laser beam ($\lambda=635$ nm). Error bars represent$\pm$one standard deviation. The laser pulse duration was 10 ms.

3.4 Transmission Measurements. The traces recorded by the oscilloscope indicated a stable pre-irradiation transmission level, followed by a large increase in transmission due to stray light from the KTP laser flash lamp, and a stable post-pulse transmission level. The change in transmission (pre- to post-laser pulse) with radiant exposure is presented in Fig. 5. A sample size of six or more was used for each data point in the graph. The data points represent the average of the sample and the error bars represent$\pm$the standard deviation. At radiant exposures of 4.0 J/cm^2 or less, the difference in transmission before and after the laser pulse was insignificant. As H_o increased from 4.0 to 5.0 J/cm^2, a significant decrease in transmission occurred. For radiant exposures greater than 5.0 J/cm^2, the transmission decrease became approximately linear with radiant exposure.

4 Discussion

4.1 Threshold Radiant Exposure for Coagulation. In experimental studies it is often assumed that coagulation onset ($\Omega=1$) corresponds to readily detectable (visible) tissue alterations. In this study, three different detection methods indicated two different threshold values: visual observation indicated that the threshold radiant exposure (H_{th}) was 3.6 J/cm^2, whereas transmission measurements and optical coherence tomography indicated that $H_{th}=4.4$ J/cm^2.

Coagulum thickness changed rapidly with H_o near the threshold radiant exposure (Fig. 5), whereas significant changes in transmission required slightly higher radiant exposures. The light transmitted through the cuvette was moderately diffuse due to the

light scattering properties of native blood ($\mu_s = 460\,\mathrm{cm}^{-1}$, g g=0.995). Coagulum formation may not have significantly increased the diffuse nature of the light propagating through the blood until the coagulum size reached a specific threshold. The scattering parameters of the blood coagulum may have been similar to that of denatured albumin ($\mu_s \sim 150\,\mathrm{cm}^{-1}$, $g = 0.8$) [20]. If this was true, for a coagulum thickness less than ~67 μm most photons underwent a single forward-scattering event in the coagulated region, whereas thicker coagula resulted in multiple scattering events which significantly altered photon trajectory.

After the initial sharp decrease in transmission in the $H_o = 5-6\,\mathrm{J/cm}^2$ range, Fig. 5 shows a more gradual change above 6 J/cm^2. This change is likely due to the fact that the beam size was decreased from 5 to 4 mm between $H_o = 6$ and 7 J/cm^2. As beam diameter decreased, the probability of light being transmitted through a fixed 6-mm-diameter aperture increased, thus reducing the rate of decrease in transmission with radiant exposure. Another decrease in slope occurs at ~9 J/cm^2 where the beam diameter was further reduced to 3 mm.

A previous study by Verkruysse et al. [14] indicated that for in vitro irradiation of blood with a 0.5 ms laser pulse ($\lambda = 586$ nm), the time at which coagulation onset occurs during the pulse is determined by when a radiant exposure corresponding to H_{th} has been delivered. Although this approach is not strictly consistent with an Arrhenius analysis, the difference between the theoretically determined onset time and that predicted using H_{th} is negligible for many processes involving short laser pulses and high damage accumulation rates (>1000 s^{-1}). In the present study, a radiant exposure equivalent to H_{th} (assuming a threshold of 4.4 J/cm^2) was delivered for the 8, 10, and 12 J/cm^2 pulses in 5.5, 4.4, and 3.7 ms, respectively (assuming a constant irradiance), and resulted in measured temperatures of 89, 90, and 99°C and computed thermal damage (Ω) levels of 0.1, 0.1, and 10.1 (at the respective times). These discrepancies indicate that thermal losses occurred during the 10 ms laser pulse, leading to reductions in temperature and thermal damage. Thus, the use of H_{th} for prediction of transient coagulation onset appears to produce only moderately accurate results for the cases studied.

4.2 Arrhenius Equation. Threshold temperatures and radiant exposures are useful for rough approximations of damage onset. However, the Arrhenius equation provides a method of quantifying thermal damage accumulation that is much more accurate and flexible. The cost of these benefits is that calculation of thermal damage at any specific location requires accurate transient temperature data and a knowledge of local tissue rate process coefficients.

The data in Fig. 3 indicate that the accuracy of the Arrhenius relation is highly dependent upon the rate process coefficients used. Threshold radiant exposures of 5.0 and 3.1 J/cm^2 were predicted using rate process coefficients for Hb and bulk skin, respectively. Thus, the results of transmission and OCT experiments indicate better agreement with predictions for Hb than those for bulk skin. However, the visually observed threshold is in better agreement with predictions based on bulk skin coefficients.

Since Lepock et al. [13] used a different technique (calorimetry) to determine the rate process coefficients for Hb, it is likely that the primary difference between the rate process coefficients for Hb and whole blood is the activation energy (E_a). The temperature data corresponding to $H_{\mathrm{th}} = 4.4\,\mathrm{J/cm}^2$ was found to predict $\Omega = 1$ when the rate process parameters found by Lepock et al. were used, with E_a reduced slightly to 448 kJ/mole (whereas data for $H_{\mathrm{th}=3.6\,\mathrm{J/cm}^2}$ indicated $E_a = 434$ kJ/mole). This alteration in E_a caused the threshold temperatures in Fig. 1 (as calculated with Eq. (2)) to shift downward while the slope of the curves remained nearly unchanged. The time–temperature relationship seen in this figure indicates that the transmission and OCT-based values are in moderately good agreement with blood constituents such as albumin and Hb. It should also be noted that these materials all have a similar threshold temperature as arterial tissue, given a 10 ms exposure time (Table 1). This is significant since it indicates that both of the primary tissue components in photothermolysis require similar temperatures to coagulate, and that these temperatures are significantly higher than previously assumed. The data in Fig. 1 corresponding to the visual observation endpoint ($H_{\mathrm{th}} = 3.6\,\mathrm{J/cm}^2$) are not in good agreement with any other data set, yet are in better agreement with the bulk skin data than any other material.

Although our results indicate that the Arrhenius equation is useful in predicting post-irradiation coagulation onset for this specific case, true validation will require corroboration of transient temperature and thermal damage data.

4.3 Coagulation Threshold Temperatures. By definition, specification of a threshold temperature (T_{th}) implies a step change in temperature and a well-defined exposure time [23]. Since the transient thermal processes investigated in this study do not have step temperature profiles, an Arrhenius approach indicates that two temperatures are useful in describing a coagulation event: an onset threshold temperature (T_{on})—the maximum temperature that occurs for a radiant exposure of H_{th}— and a transient threshold (T_{tr})—the temperature at the instant of coagulation onset (for an event during which coagulation occurs during the laser pulse).

Interpolating from the data in Fig. 2, the threshold radiant exposure of 4.4 J/cm^2 corresponds to a maximum radiometric temperature of 90±3°C (T_{on}). This result is in reasonable agreement with the threshold temperature for a 10 ms step temperature change in blood constituents such as albumin and Hb (Table 1, lines 5 and 8), but significantly higher than the 60°C–80°C used to predict vessel necrosis in theoretical models of pulsed laser treatment of vascular lesions [1,28,29]. However, it should be noted that the maximum temperature corresponding to a radiant exposure of 3.6 J/cm^2 was 78.5°C.

For radiant exposures significantly greater than $H_{\mathrm{th}} = 4.4\,\mathrm{J/cm}^2$, T_{on} was reached during the laser pulse, but since coagulation at T_{on} requires a finite exposure duration, greater temperatures (and a greater damage accumulation rate, $d\Omega/dt$) were produced before coagulation occurred (at T_{tr}). Since transmission and coagulum thickness data were not collected transiently during the laser pulse, it is difficult to identify T_{tr} directly from experimental results. However, using the rate process coefficients indicated in the previous section for $H_{\mathrm{th}} = 4.4\,\mathrm{J/cm}^2$, coagulation onset for $H_o = 8.0$, 10.0, and 12.0 J/cm^2 was predicted to occur at temperatures of 95°C–99°C. The corresponding temperature range determined for $H_{\mathrm{th}} = 3.6\,\mathrm{J/cm}^2$, was 82°C–86°C.

4.4 Thermally Induced Changes in Optical Properties. The OCT images in Fig. 4 clearly indicate the increased level of light scattering induced by thermal coagulation of blood. These findings are in agreement with previous investigations, which have indicated that thermal damage of blood constituents results in an increase in scattering [10,15]. Although the transient effects of light scattering were not documented in this study, it is likely that the coagulated region increased in thickness both during and after the laser pulse in a manner predictable by rate process kinetics [19].

Since blood contains various proteins, which have different coagulation thresholds, it is possible that multiple changes in optical properties occurred. Results such as the indication of slight blood discoloration at $H_o = 3.6\,\mathrm{J/cm}^2$ may have been a result of scattering brought on by denaturation of blood constituents which are less thermally stable, such as erythrocyte membrane proteins [10]. However, Arrhenius data (Fig. 1) indicate that membrane proteins have a higher threshold temperature than other blood components for short exposure times.

For radiant exposures above 5.0 J/cm^2, Fig. 2 indicates that when measured temperatures of 70°C or greater are reached, the slope of the temperature curve decreases, then becomes relatively constant above 100°C. A simple one-dimensional transient thermal model which included convection, conduction and a Beer's

law-based source term (but not evaporative cooling nor changes in optical properties) was developed. Simulations indicated a nearly linear temperature rise, without the aforementioned changes at 70°C and 100°C. Therefore, other mechanisms need to be considered. In this temperature regime, heat loss by water vaporization is a significant factor (see Section 4.6). However, dynamic changes in optical properties may also play a significant role in the transition near 100°C as well. The change in slope is nearly simultaneous with the onset of coagulation as predicted by the Arrhenius relation using the rate process coefficients of Hb (Fig. 3). Coagulation-induced changes produce an increase in scattering, which should increase the rate of temperature rise. Such an increase was not noted, possibly because the increase in scattering was small in comparison to the high absorption coefficient.

Dynamic changes in absorption, which may also play a role in the transient changes seen in the temperature distribution, are not well understood. A dynamic decrease in transmission was noted by Verkruysse et al. [14] during pulsed laser irradiation of blood (at $\lambda = 586$ nm). Temperature-dependent changes in Hb absorption were indicated to be the dominant mechanism; however, dynamic changes in scattering were not accounted for thoroughly. At wavelengths for which there is a large disparity in absorption between Hb and HbO_2 (such as 586 or 1064 nm), significant transmission changes may result from thermally induced deoxygenation of HbO_2 [15]. Since the difference between μ_a for Hb (185.1 cm^{-1}) and HbO_2 (228.8 cm^{-1}) is less than 20 percent at $\lambda = 532$ nm, it is not likely that this effect played a significant role during laser irradiation [30]. However, there is an order of magnitude difference in absorption coefficient of blood at $\lambda = 635$ nm between HbO_2 (2.2 cm^{-1}) and Hb (22 cm^{-1}). Therefore, the transmission measurements presented in Fig. 5 may have been affected by changes in absorption as well as scattering.

4.5 Coagulum Size and Consistency. The variation in coagulum thickness with radiant exposure (Fig. 5) shows a steep initial slope followed by a more moderate slope, which continues until ablation. The second phase of the curve indicates a region for which changes in coagulum depth occur in nearly direct proportion to changes in radiant exposure. Similar trends have been noted in a previous study of Holmium:YAG irradiation of albumen [18].

As shown in Fig. 5, the maximum blood coagulum thickness recorded was 175 μm ($H_o = 10$ J/cm^2). At a depth of 175 μm, only 1.8 percent of the initial fluence remains if the blood is highly oxygenated (3.9 percent if de-oxygenated). Therefore, it is likely that axial heat diffusion caused the coagulated region to be thicker than if the process were thermally confined. It is also possible that convective (pressure or temperature-driven) flow may have played a role.

The transition from a region of disconnected (or weakly bonded), denatured proteins to an aggregated coagulum appears to have taken place between radiant exposures of 8.0 and 10.0 J/cm^2, although it was not detectable by OCT imaging. If a threshold radiant exposure for aggregation of 9.0 J/cm^2 is assumed, the threshold temperature would be ~115°C, and the resulting thermal damage, ~1000 using the Arrhenius equation and rate coefficients of Hb (Table 1, line 8). However, accurate prediction will not likely be accurately achieved using the rate process coefficients for hemoglobin. If aggregation can indeed be modeled as a rate process, experimental determination of a novel set of rate process coefficients will be necessary.

The finding of blood coagula in various stages of aggregation corresponding to radiant exposure level is in agreement with previous findings [6], which indicated that the threshold for embolized coagulum formation was much lower than the radiant exposure required for formation of a flow-stopping coagulum. The mechanism of transition from an unconnected solution of denatured molecules to a strongly bonded coagulum is very significant not only for arresting flow in blood vessels but for other applications such as forming patent anastomoses with a laser, yet it is still not well understood. It is likely that the primary mechanism is either an increase in the concentration of denatured molecules due to additional thermal damage or evaporative water loss, which decreases the intermolecular space, thus facilitating bond formation. In order to achieve a better understanding of this process, it will be necessary to study the molecular composition and microscopic morphology of coagula.

4.6 Effect of Phase Change. Radiometric temperature measurements provided evidence of several significant dynamic mechanisms. In Fig. 2, the linear slope for the lowest radiant exposure indicates a situation in which minimal dynamic changes occur. For higher H_o values, maximum temperatures rose above 70°C, vapor production was observed, and the rate of temperature rise decreased. These results indicate that phase change became significant at about 70°C. This is in fair agreement with the literature, which indicates that for CW processes, evaporation becomes significant at about 60°C, and increases exponentially with temperature [15,31,32]. Therefore, one would expect that as temperatures exceeded 100°C, the rate of temperature rise would continue to decrease, whereas in fact, it became relatively constant (Fig. 2). For CW irradiation, Halldorsson [15] reported a significant increase in the rate of temperature rise above 95°C, which he explained as being due to desiccation of the surface blood. Therefore, an exponential increase in evaporation rate, followed by a reduction in cooling due to desiccation, may help explain the measured temperature distributions.

The threshold radiant exposure for ablation determined in this study was ~12 J/cm^2 and the corresponding maximum surface temperature (during nonablative irradiation) was 145°C. At this temperature water has a saturation pressure of greater than 4 atm [33]. In order to establish whether the maximum surface temperature was also the maximum tissue temperature, it is necessary to consider two possible scenarios proposed in the literature. Evaporative cooling may have acted to moderate the heating rate at temperatures greater than 60°C. As the tissue became desiccated—likely near 100°C—the cooling mechanism was reduced and the rate of temperature rise increased sharply near the surface, leading to ablation [23]. This sharp increase is not seen in Fig. 2, possibly because desiccation caused a reduction in emissivity, resulting in an underestimation of the temperatures in the superficial blood layers. If this description of the ablation process is accurate, then the surface temperature was the maximum tissue temperature. Alternatively, surface heat loss and a layer of highly absorbent, highly scattering coagulum may have produced a subsurface temperature peak which in turn led to phase change and a corresponding subsurface peak in pressure. When internal pressures exceeded the restraining forces (e.g., blood surface tension, coagulum tensile strength), ablation occurred [34]. If a subsurface temperature peak occurred deeper than 20 μm, then the measured temperatures may represent a significant underestimation (Fig. 2).

5 Conclusions

Pulsed KTP laser-induced thermal damage in whole blood was investigated in vitro. A progression of events occurred with increasing radiant exposure: evaporation, coagulation onset, aggregated coagulum formation, and ablation. Both coagulation and ablation were indicated to occur at higher temperatures than typically assumed by previous theoretical models of laser treatment of cutaneous vascular lesions. Phase change was shown to play a primary role, leading to surface heat loss (and possibly desiccation of the coagulum) as well as ablation. The Arrhenius equation was indicated to be valid for predicting pulsed laser-induced coagulation of blood, with the rate process coefficients for hemoglobin indicating better agreement with experimental data than the commonly used bulk skin coefficients.

Acknowledgments

The authors would like to thank Dr. John Pearce and Dr. James Lepock for significant discussions regarding this research. Fund-

ing for this research was provided in part by grants from the Air Force Office of Scientific Research through MURI from DDR&E (F49620-98-1-0480), the Office of Naval Research Free Electron Laser Biomedical Science Program (N00014-91-J-1564), and the Albert W. and Clemmie A. Caster Foundation. A. J. Welch is the Marion E. Forsman Professor of Electrical and Computer Engineering.

Nomenclature

A = frequency factor, 1/s
CW = continuous wave
E_a = activation energy, J/mole
Ho = holmium
H_o = radiant exposure, J/cm^2
H_{th} = threshold radiant exposure, J/cm^2
KTP = potassium–titanyl–phosphate
n = index of refraction
Nd = neodymium
OCT = optical coherence tomography
T = temperature, °C or K
T_{th} = threshold temperature
T_{on} = onset threshold temperature
T_{tr} = transient threshold temperature
YAG = yttrium–aluminum–garnet
ε = emissivity
λ = wavelength, nm
τ_p = pulse duration, ms
Ω = thermal damage coefficient

References

[1] Van Gemert, M. J. C., Welch, A. J., Pickering, J. W., and Tan, O. T., 1995, ''Laser Treatment of Port Wine Stains,'' in *Optical-Thermal Response of Laser-Irradiated Tissue*, A. J. Welch and M. J. C. Van Gemert, eds., Plenum Press, New York.
[2] Boergen, K. P., Birngruber, R., and Hillenkamp, F., 1979, ''Experimental Studies on Argon Laser Coagulation of Small Blood Vessels,'' Mod. Probl. Ophthalmol., **20**, pp. 174–183.
[3] Nishioka, N. S., Tan, O. T., Bronstein, B. R., Farinelli, W. A., Richter, J. M., Parrish, J. A., and Anderson, R. R., 1988, ''Selective Vascular Coagulation of Rabbit Colon Using a Flashlamp-Excited Dye Laser Operating at 577 Nanometers,'' Gastroenterology, **95**, pp. 1258–1264.
[4] Poppas, D. P., Wright, E. J., Guthrie, P. D., Shlahet, L. T., and Retik, A. B., 1996, ''Human Albumin Solders for Clinical Application During Laser Tissue Welding,'' Lasers Surg. Med., **19**, pp. 2–8.
[5] Hunter, J. G., 1989, ''Endoscopic Laser Applications in the Gastrointestinal Tract,'' Surg. Clin. North Am., **69**, No. 6, pp. 1147–1166.
[6] Barton, J. K., Welch, A. J., and Izatt, J. A., 1998, ''Investigating Pulsed Dye Laser-Blood Vessel Interaction With Color Doppler Optical Coherence Tomography,'' Opt. Express (http://epubs.osa.org/opticsexpress/), **3**, No. 6, pp. 251–256.
[7] Barton, J. K., Hammer, D. X., Pfefer, T. J., Lund, D. J., Stuck, B. E., and Welch, A. J., 1999, ''Simultaneous Irradiation and Imaging of Blood Vessels During Pulsed Laser Delivery,'' Lasers Surg. Med., **24**, pp. 237–243.
[8] Guyton, A. C., 1991, *Textbook of Medical Physiology*, W. B. Saunders Co., Philadelphia.
[9] Kapit, W., Macey, R. I., and Meisami, E., 1987, *Physiology Coloring Book*, Harper Collins, Cambridge.
[10] Nilsson, A. M. K., Lucassen, G. W., Verkruysse, W., Andersson-Engels, S., and Van Gemert, M. J. C., 1997, ''Changes in Optical Properties of Human Whole Blood *in Vitro* Due to Slow Heating,'' Photochem. Photobiol., **65**, pp. 366–373.
[11] Abela, G. S., Crea, F., Smith, W., Pepine, C. J., and Conti, C. R., 1985, ''*In Vitro* Effects of Argon Laser Radiation on Blood: Quantitative and Morphologic Analysis,'' J. Am. Coll. Cardiol., **5**, pp. 231–237.
[12] Thomsen, S., 1991, ''Pathologic Analysis of Photothermal and Photomechanical Effects of Laser-Tissue Interactions,'' Photochem. Photobiol., **53**, pp. 825–835.
[13] Lepock, J. R., Frey, H. E., Bayne, H., and Markus, J., 1989, ''Relationship of Hyperthermia-Induced Hemolysis of Human Erythrocytes to the Thermal Denaturation of Membrane Proteins,'' Biochim. Biophys. Acta, **980**, pp. 191–201.
[14] Verkruysse, W., Nilsson, A. M. K., Milner, T. E., Beek, J. F., Lucassen, G. W., and Van Gemert, M. J. C., 1998, ''Optical Absorption of Blood Depends on Temperature During a 0.5 ms Laser Pulse at 586 nm,'' Photochem. Photobiol., **67**, No. 3, pp. 276–281.
[15] Halldorsson, T., 1981, ''Alteration of Optical and Thermal Properties of Blood by Nd:YAG Laser Irradiation,'' presented at *The 4th Congress of The International Society for Laser Surgery*.
[16] Theis, J. H., Lee, G., Ikeda, R. M., Stobbe, D., Ogata, C., Lui, H., and Mason, D. T., 1983, ''Effects of Laser Irradiation on Human Erythrocytes: Considerations Concerning Clinical Laser Angioplasty,'' Clin. Cardiol., **6**, pp. 396–398.
[17] Flock, S., Smith, L., and Waner, M., 1993, ''Quantifying the Effects on Blood of Irradiation With Four Different Vascular-Lesion Lasers,'' Proc. SPIE, **1882**, pp. 237–242.
[18] Asshauer, T., Delacretaz, G. P., and Rastegar, S., 1996, ''Photothermal Denaturation of Egg White by Pulsed Holmium Laser,'' Proc. SPIE, **2681**, pp. 120–124.
[19] Pfefer, T. J., Chan, K. F., Hammer, D. X., and Welch, A. J., 1998, ''Pulsed Holmium:YAG-Induced Thermal Damage in Albumen,'' Proc. SPIE, **3254**, pp. 192–202.
[20] McNally, K. M., 1998, ''Optical and Thermal Studies of Laser-Solder Tissue Repair *in Vitro*,'' Ph.D. Thesis, Macquarie University, Sydney, Australia.
[21] Henriques, F. C., and Moritz, A. R., 1947, ''Studies In Thermal Injury. I. The Conduction of Heat to and Through Skin and the Temperature Attained Therein. A Theoretical and an Experimental Investigation,'' Am. J. Pathol., **23**, pp. 531–549.
[22] Moritz, A. R., and Henriques, F. C., 1947, ''Studies in Thermal Injury II. the Relative Importance of Time and Surface Temperature in the Causation of Cutaneous Burns,'' Am. J. Pathol., **23**, pp. 695–720.
[23] Pearce, J., and Thomsen S., 1995, ''Rate Process Analysis of Thermal Damage,'' in: *Optical-Thermal Response of Laser-Irradiated Tissue*, A. J. Welch and M. J. C. Van Gemert, eds. Plenum Press, New York.
[24] Yang, Y., Welch, A. J., and Rylander, H. G., 1991, ''Rate Process Parameters of Albumen,'' Lasers Surg. Med., **11**, pp. 188–190.
[25] Henriques, F. C., 1947, ''Studies in Thermal Injury. V. The Predictability and Significance of Thermally Induced Rate Processes Leading to Irreversible Epidermal Injury,'' Arch. Pathol., **43**, pp. 489–502.
[26] Sturesson, C., and Andersson-Engels, S., 1996, ''Mathematical Modelling of Dynamic Cooling and Pre-heating Used to Increase the Depth of Selective Damage to Blood Vessels in Laser Treatment of Port Wine Stains,'' Phys. Med. Biol., **41**, pp. 413–428.
[27] Pfefer, T. J., Barton, J. K., Smithies, D. J., Milner, T. E., Nelson, J. S., Van Gemert, M. J. C., and Welch, A. J., 1999, ''Modeling Laser Treatment of Port Wine Stains With a Computer-Reconstructed Biopsy,'' Lasers Surg. Med., **24**, pp. 151–166.
[28] Smithies, D. J., Butler, P. H., Day, W. A., and Walker, E. P., 1995, ''The Effect of the Illumination Time When Treating Port-Wine Stains,'' Las. Med. Sci., **10**, pp. 93–104.
[29] De Boer, J. F., Lucassen, G. W., Verkruysse, W., and Van Gemert, M. J. C., 1996, ''Thermolysis of Port-Wine-Stain Blood Vessels: Diameter of a Damaged Blood Vessel Depends on the Laser Pulse Length,'' Las. Med. Sci., **11**, pp. 177–180.
[30] Zijlstra, W. G., Buursma, A., and Meeuwsen-Van Der Roest, W. P., 1991, ''Absorption Spectra of Human Fetal and Adult Oxyhemoglobin, Deoxyhemoglobin, Carboxyhemoglobin, and Methemoglobin,'' Clin. Chem., **37**, pp. 1633–1638.
[31] Torres, J. H., Motamedi, M., Pearce, J. A., and Welch, A. J., 1993, ''Experimental Evaluation of Mathematical Models for Predicting the Thermal Response of Tissue to Laser Irradiation,'' Appl. Opt., **32**, No. 4, pp. 597–606.
[32] Incropera, F. P., and DeWitt, D. P., 1996, *Fundamentals of Heat and Mass Transfer*, 4th ed., Wiley, New York.
[33] Howell, J. R., and Buckius, R. O., 1987, *Fundamentals of Engineering Thermodynamics*, McGraw-Hill, New York.
[34] LeCarpentier, G. L., Motamedi, M., McMath, L. P., Rastegar, S., and Welch, A. J., 1993, ''Continuous Wave Laser Ablation of Tissue: Analysis of Thermal and Mechanical Events,'' IEEE Trans. Biomed. Eng., **40**, No. 2, pp. 188–199.
[35] Agah, R., Pearce, J. A., Welch, A. J., and Motamedi, M., 1994, ''Rate Process Model for Arterial Tissue Thermal Damage: Implications for Vessel Photocoagulation,'' Lasers Surg. Med., **15**, pp. 176–184.
[36] Moussa, N. A., Tell, E. N., and Cravalho, E. G., 1979, ''Time Progression of Hemolysis of Erythrocyte Populations Exposed to Supraphysiological Temperatures,'' ASME J. Biomech. Eng., **101**, pp. 213–217.
[37] Barnes, F. S., 1974, ''Biological Damage Resulting From Thermal Pulses,'' in: *Laser Applications in Medicine and Biology*, M. L. Wolbarsht, ed., Plenum Press, New York.